

## Simulation of discrete electromagnetic propagation model for atmospheric effects on mobile communication

Şaban Selim ŞEKER,<sup>1</sup> Fulya KUNTER<sup>2,\*</sup>

<sup>1</sup>Department of Electrical and Electronics Engineering, Faculty of Engineering, Boğaziçi University, Bebek, İstanbul, Turkey

<sup>2</sup>Department of Electrical and Electronics Engineering, Faculty of Engineering, Marmara University, Kadıköy, İstanbul, Turkey

Received: 05.04.2012

Accepted: 08.06.2012

Published Online: 24.10.2013

Printed: 18.11.2013

**Abstract:** Wireless communication has become an important part of our lives, and atmospheric effects are one of the ultimate factors affecting quality of communication and satellite systems. In this study the attenuation in mobile communication due to atmospheric events like snow and rain is simulated using the discrete propagation model. In this work, spherical raindrop and oblate spheroid raindrop modeling are used. To check the validity of simulations, the commonly used and accepted ITU-R rain model is used. Oblate spheroid raindrop modeling produces results that are more compatible with ITU-R results, especially at frequencies higher than 50 GHz. At lower frequencies, both raindrop shapes produce results that are not compatible with ITU-R results. Moreover, attenuation of snow is simulated for different types using the discrete propagation model and uniform distribution of snowflakes. The attenuation of vegetation is also simulated. It is found that snow attenuation is higher than rain attenuation, specifically because of the differences in particle size. In all simulations, frequencies of GSM communication of 900 MHz, 1800 MHz, and 2270 MHz are used for calculation and discussion of the results.

**Key words:** Propagation, atmospheric effects, mobile communication, simulation

### 1. Introduction

The rapid growth of mobile services has highlighted a need for estimating propagation factors. Snow and rain attenuations are considered as dominant factors. Atmospheric effects play a major role in the designing of all of the links. Raindrops and snowflakes absorb and scatter radio waves, leading to signal attenuation and reduction of the mobile system availability and reliability. Propagation impairments produced by the rain and snow are limiting factors for the effective use of mobile systems. It is known that the important difference between mobile UMTS and GSM systems in terms of radio propagation is the difference in the carrier spacing, which is 5 MHz in UMTS systems and 200 kHz for GSM systems. For this reason, UMTS systems are more vulnerable to atmospheric effects than GSM systems. This is why mobile system predictions should be as accurate as possible. This discrete model will be a good preliminary design tool for both terrestrial and earth-satellite mobile links and will also provide a broad idea of rain and snow attenuation for microwave engineers.

Due to new needs and developments, system designers are interested in frequencies above 10 GHz, and rain attenuation is one of the important parameters in system design. For this reason, the International Telecommunication Union (ITU) recommends an expression for rain attenuation at a given frequency and

\*Correspondence: [fulya.kunter@marmara.edu.tr](mailto:fulya.kunter@marmara.edu.tr)

rain rate [1–3]. However, although this simple model is widely used in telecommunications, since the drop size distribution changes on different continents or in different districts, the ITU model may not be representative of weather around the world. Therefore, a modification of the ITU or a new model is needed to gain a deeper understanding and to improve the mobile communication in a specific area. The main objective of this work is to simulate the attenuation in mobile communication at frequencies used in Turkey such as 900, 1800, and 2270 MHz due to atmospheric events like snow and rain by using the discrete propagation model [4].

Clouds can be categorized as hydrosols, which are liquid water droplets having a diameter of less than 10 mm [5]. Cloud attenuation becomes especially significant at frequencies higher than 20 GHz [6]. Cloud attenuation depends on frequency, liquid water content of the cloud, elevation angle, types of the cloud, shape and size of the cloud, cloud base height, and the present weather. Moreover, attenuation increases as temperature decreases [7]. Since cloud attenuation depends on many factors that are hard to observe and identify or classify, modeling of cloud attenuation is relatively more complex.

Direct rain attenuation at each frequency and location is not available; therefore, prediction and modeling should be done to reach the best estimate for each frequency and location. There are 2 main classes of methods used in rain attenuation prediction: the empirical method and the physical method. The physical method focuses on reproducing the physical behavior of factors involved in the process; however, it is not commonly practiced since the access to input parameters is limited. The empirical method focuses on sets of data taken from different climatic zones, and it is the most preferred methodology. However, there are some other input parameters needed for empirical methodology. One of these input parameters is rainfall rate, which is provided by meteorological agencies, national weather bureaus, and researchers [7–9].

Snow can be considered as a combination of water, ice crystals, and air molecules. It should be noted that snow attenuation is not negligible since it could be more serious than attenuation due to rain [10,11]. While rain causes attenuation of 20–30 dB/km under a certain rain rate, snow can cause attenuation of up to 45 dB/km. Snow attenuation depends on the size of the snowflake, water content, and snowfall rate.

## 2. Theoretical background

There are many methods that have been developed by researchers, but only the most commonly used one, the ITU-R rain model and discrete theoretical model, will be discussed in this work.

### 2.1. ITU-R model

The ITU-R rain model is the most preferred and accepted model internationally. It was created and accepted in 1982; however, it is being constantly reviewed and updated as better understanding of rain attenuation is attained.

Again, rain attenuation from rain rates is desired to be calculated. Therefore, Eq. (1) is valid:

$$A_T(dB) = aR^b L(R), \quad (1)$$

where  $R$  is the rain rate,  $a$  is the frequency-dependent attenuation coefficients,  $b$  is the frequency-dependent attenuation coefficients, and  $L(R)$  is the effective path length parameter as a function of  $R$ . Values of  $a$  and  $b$  are determined as functions of frequency in the range of 1 to 1000 GHz [1].

**2.2. Discrete model**

We considered the problem of scattering of a time-harmonic electromagnetic wave from  $N$  discrete lossy dielectric scatterers, which have random positions and orientations in a volume  $V$ , which represents rain or snow. Let identical scatterers have volume  $V_p$ , relative dielectric  $\epsilon_r$ , radius  $R$ , and a scatterer density that is taken as a constant value  $\rho$  for this study. The surrounding medium is considered to be free space.

In this way, one can obtain a mean field equation from Maxwell’s equations, assuming the incident field on each scatterer is in itself the mean field (Foldy approximation). By using this approximation along with an assumed sparse distribution of scatterers, which indicates the fractional volume  $\delta = \rho V_p$  to be very small, the component of electric fields  $E_{\alpha\beta}$  can be easily obtained [4].

$$E_{\alpha\beta} = \exp(iK_{\alpha\beta}L) \quad \alpha, \beta \in (h, v) \tag{2}$$

Here  $K_{\alpha\beta}$  is the effective propagation constant and is given by:

$$K_{\alpha\beta} = k_0 + \frac{2\pi\rho}{k_0} \bar{f}_{\alpha\beta}(\underline{i}, \underline{i}) \quad \alpha, \beta \in (h, v). \tag{3}$$

The attenuation and phase coefficients and equivalent permittivity of the medium are given as:

$$A_{v,h} = 8,686 \text{Im}(K_{v,h}) \times 10^3 \text{ dB/km}, \tag{4}$$

$$\varphi_{v,h} = \frac{180}{\pi} \text{Re}(K_{v,h}) \times 10^3 \text{ deg/km}, \tag{5}$$

$$A_{pp} = 8,686\lambda\rho \text{Im}(\bar{f}_{pp}) \quad p \in \{h, v\}, \tag{6}$$

where  $k_0 = \omega\sqrt{\epsilon_0\mu_0}$  is the free-space propagation constant and  $\bar{f}_{\alpha\beta}(\underline{i}, \underline{i})$  is the average of the forward dyadic scattering amplitude of the raindrop with given shape and dielectric constant. The average is taken over appropriate distribution variables such as size and orientation angle. The effective propagation constant in the multicomponent environment is expressed in terms of the forward-scattering amplitude of its individual components of medium, as follows:

$$k_0 + \frac{2\pi}{k_0} \{ \rho_t \bar{f}_{pp}^{(t)} + \rho_b \bar{f}_{pp}^{(b)} + \rho_n \bar{f}_{pp}^{(n)} + \rho_l \bar{f}_{pp}^{(l)} \}, \tag{7}$$

where  $\bar{f}_{pp}^{(t)}, \bar{f}_{pp}^{(b)}, \bar{f}_{pp}^{(n)}$ , and  $\bar{f}_{pp}^{(l)}$  are the average forward-scattering amplitudes for thick cylinders (t), thin cylinders (b), needles (n), and disks (l), respectively.

The specific attenuation for the mean field can be obtained from the above equations as:

$$A_{pp} = 8.686\lambda \text{Im} \{ \rho_t \bar{f}_{pp}^{(t)} + \rho_b \bar{f}_{pp}^{(b)} + \rho_n \bar{f}_{pp}^{(n)} + \rho_l \bar{f}_{pp}^{(l)} \}, p \in \{h, v\}. \tag{8}$$

In the derivation of the above result, the assumption was made that the plane wave is scattered only once (single scattering) by the particles before reaching the receiver. When the scattering coefficients of the particles and the particle density are small, contributions to the scattered wave by second-, third-, and higher-order scattering may be ignored. There are cases, however, where the scattering coefficients of the scatterer are large and the multiple scattering contributions cannot be ignored.

In this model it is assumed that the drop axes align with the polarization directions, so no cross-polarization exists in this coordinate system. Thus, the propagation coefficients are given in the preferred direction where no coupling exists. In the physical problem, the drops will not in general align this way. Actually, it is the representative drop in its representative orientation that we are dealing with, and, in general, this drop will not align with the polarization directions. We may rotate to the preferred direction where cross-terms are not zero.

**3. Basic scattering formulation**

Consider a plane electromagnetic wave incident on an arbitrarily oriented dielectric oblate spheroid with its semiaxis (a, b, c) aligned along the coordinates (x', y', z') of a local frame related to the principal frame (x, y, z) through the Euler angles (θ, φ, γ) of rotation. The incident plane wave is assumed to have polarization q<sub>0</sub> and to be propagating in the i direction.

$$E_{inc}(x) = q^0 E_0 e^{ik_0 i_0 x}, \tag{9}$$

where E<sub>0</sub> is the magnitude of the incident wave, k<sub>0</sub> = ω√ε<sub>0</sub> μ<sub>0</sub>, and i is the incident direction of incoming wave.

The scatterer, which is assumed to be homogeneous and isotropic, is characterized by constitutive parameters: permittivity ε<sub>0</sub>ε<sub>r</sub> and permeability μ<sub>0</sub> of the dielectric material. The surrounding medium is considered to be free space. Under the quasistatic approximation, the internal field of a spheroid is obtained as given below:

$$E_{int}(x', q) = E_0 \{ K_3(q^0 \cdot r^0) r^0 + K_1(q^0 \cdot \theta^0) \theta^0 + K_2(q^0 \cdot \varphi^0) \varphi^0 \} e^{ik_0 i \cdot x'}, \tag{10}$$

where r<sup>0</sup>, θ<sup>0</sup>, and φ<sup>0</sup> are spherical unit vectors in the principal frame and

$$K_1 = \frac{1}{1 + L_1 \Delta}, \quad K_2 = \frac{1}{1 + L_2 \Delta}, \quad K_3 = \frac{1}{1 + L_3 \Delta} \\ \Delta = \epsilon_r - 1 \tag{11}$$

$$L_1 = \int_0^\infty \frac{abcds}{2(s + a^2)^{3/2}(s + b^2)^{1/2}(s + c^2)^{1/2}} \cdot$$

The same formula with cyclical changes for L<sub>2</sub> and L<sub>3</sub> can be written [12], and the scattering amplitude is obtained as:

$$f(\theta^0, i^0, q) = \frac{k_0^2 \Delta}{4\pi} V_p (\underline{I} - \theta^0 \theta^0) \cdot E, \tag{12}$$

where

$$E = E_0 q^0 \cdot \{ K_3 r^0 r^0 + K_1 \theta^0 \theta^0 + K_2 \varphi^0 \varphi^0 \}. \tag{13}$$

For symmetric elliptical scatterers (t = 2c),

$$V_p = \frac{4\pi b}{k_0^2 V_x V_y} \sin\left(\frac{k_0 t V_z}{2}\right) \times \left[ \sum_{n=0}^\infty (-1)^n \left(\frac{k_0 b^2 V_y^2}{a V_x}\right) J_{n+1}(k_0 a V_x) \right], \tag{14}$$

where J<sub>n</sub>(x) is the Bessel function of the first kind of order n. Equations for the internal field and scattering amplitude are in their most general form. This method represents a generalization of the Rayleigh–Gans approximation. The parameters V<sub>x</sub>, V<sub>y</sub>, and V<sub>z</sub> are trigonometric expressions and are given in [13].

**4. Numerical calculations and contributions**

The theoretical model will now be used to calculate specific attenuations. For the computer program, input parameters are from [4, 10]. The rain shape is spherical and the distribution is uniform. After choosing input values, attenuation versus frequency is calculated for different  $R_i$  (mm/h), as seen in Figure 1. The rainfall rate  $R_i$  (mm/h) for the drops with a mean diameter  $D_i$  within  $\Delta D_i$  in channel  $i$  is calculated as follows:

$$R_i = \frac{2\Pi}{1000} \sum_i D_i^3 n_i, \tag{15}$$

where  $n_i$  is the number of drops in channel  $i$ . The experimental data for  $R_i$  are obtained from [7]. Comparisons with experimental results of [7] and ITU-R are very good, but there is a difference of a few decibels due to the fact that the theoretical calculation uses Rayleigh–Gans theory and not Mie’s.

The influence of the temperature of raindrop water is very weak, and the value of temperature may be neglected in estimating rainfall attenuation. Because of that, the temperature is assumed to be 20 °C in this work [6–10].

The imaginary part of the equivalent relative permittivity of rain using the same parameter of Figure 1 is illustrated in Figure 2. The real part of the equivalent permittivity of rain is around 1.

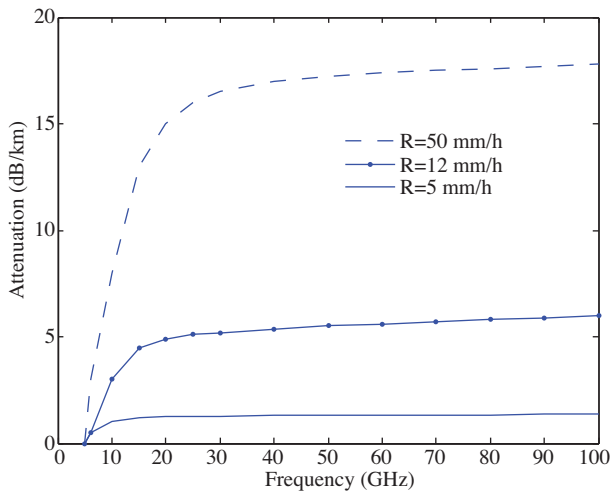


**Figure 1.** Attenuation values for various rainfall rates.

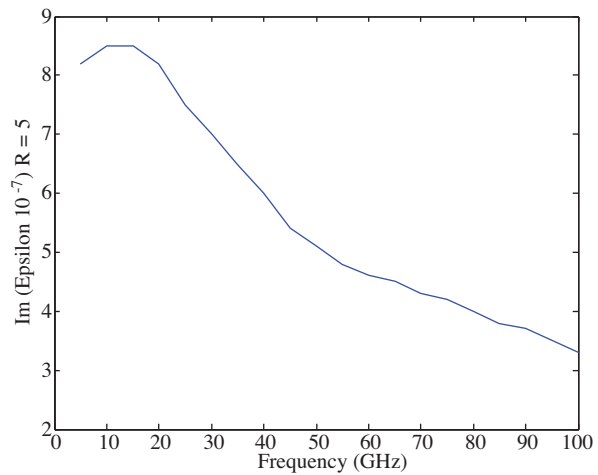


**Figure 2.** Imaginary part of equivalent permittivity of rain.

**4.1. Extension of rain attenuation**

In the discrete model, rain attenuation was observed and raindrops were considered to be spherical particles. In a literature survey, it was observed that rain particles are sometimes modeled as ellipsoids, especially disk-shaped oblate spheroids.

In the extension of the previous studies, a discrete model is realized while the raindrop shape is chosen to be an oblate spheroid that has 3 perpendicular axes, which are denoted by  $a$ ,  $b$ , and  $c$ , and they have the following relation:  $a = b > c$ .

The volume of the oblate spheroid can be calculated using the following relation:

$$V = \frac{4}{3}abc. \tag{16}$$

Previously, raindrops were modeled as a sphere by using uniform distribution for simplicity, and inputs were given as in [4–6].

Oblate spheroids are modeled having the same length on 2 axes but with the third axis being 0.6 of the length of the other axes. Due to differences in calculation, a 4/3 term is also involved in the length section to prevent complications. Therefore:  $a = b > c$ ,  $c = 0.6a = 0.6b$ , and  $length = \frac{4}{3}c$ .

Attenuation of rain for the sphere against the oblate spheroid is given in Figures 3 Figure 4. It can be observed clearly that the sphere model has a higher attenuation (dB/km) compared to the oblate model.

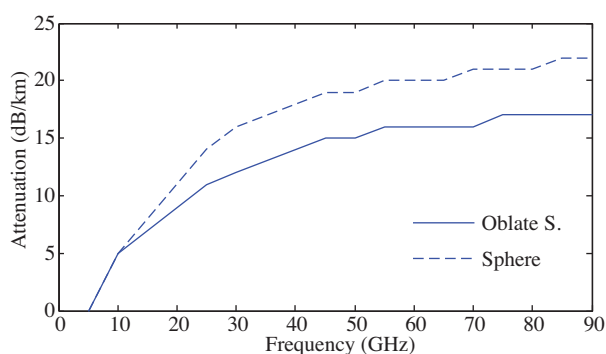


**Figure 3.** Attenuation of rain (sphere vs. oblate spheroid).

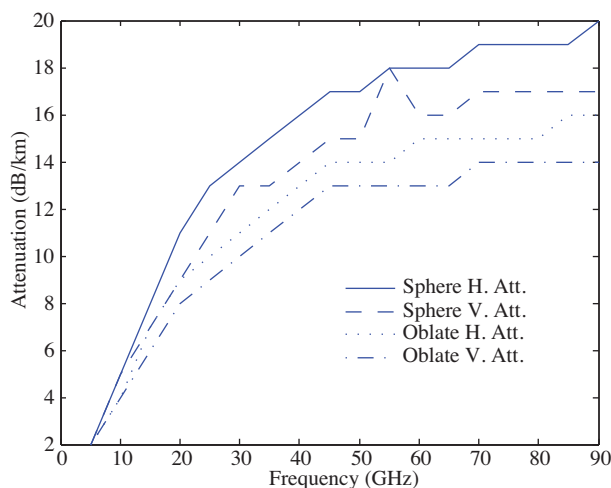


**Figure 4.** Horizontal and vertical attenuation of rain (sphere vs. oblate spheroid).

Note that both lines have a very similar trajectory. However, their magnitudes differ, especially when frequency exceeds 10 GHz. Horizontal and vertical attenuations are investigated in detail in Figure 4.

Figure 4 offers a much more clear understanding of the attenuation in terms of polarization and shape. In both sphere and oblate spheroid models of raindrops, horizontal attenuation is higher than vertical attenuation. However, the difference between horizontal and vertical attenuation values is higher in spherical model.

This can be explained in terms of the oblate sphere’s orientation being in the horizontal plane, as in the cylinder case shown in [4]. It was shown in [4] that when the diameter of a disk is between 20  $\mu$ m and 20 mm, horizontal attenuation is higher than vertical attenuation; however, outside of this zone, vertical attenuation is higher than horizontal attenuation. Since the diameters used in this study were around 10 mm to 20 mm, findings of the simulation support the previous findings of [14,15].

Attenuation levels in frequencies used in Turkey were investigated through simulations. The outcomes of the simulation can be seen in Figure 5. These simulations of rain attenuation computation by using discrete modeling depict that as the frequency increases, attenuation levels increase. However, there is no linear relation between frequency and attenuation: when the frequency is doubled from 900 MHz to 1800 MHz, attenuation increases approximately by half of the initial value.

#### 4.2. Comparison with ITU-R rain model

To be able to decide whether the oblate spheroid model or the sphere model is more convenient for modeling rain, a comparison was made with the ITU-R Rain Model [1].

For comparison purposes, attenuation at a rain rate of 50 mm/h is used, since this is the rate used in the discrete model. Moreover, at 50 mm/h, it is easier to see the changes in attenuation as frequency changes compared to slower rain rates, since the effect of change is magnified. In Figure 6, the comparison of the discrete and ITU-R rain models can be seen clearly.

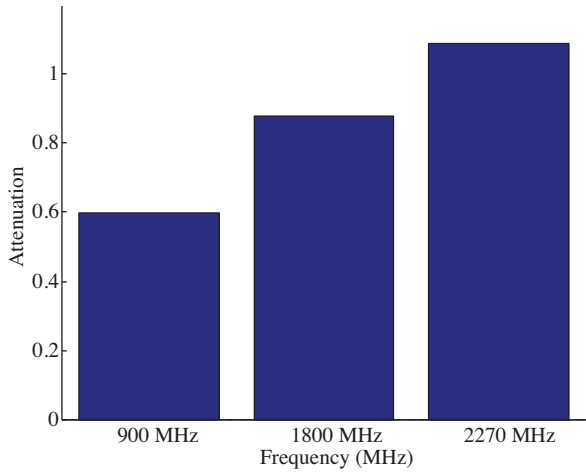


**Figure 5.** Rain attenuation at 900 MHz, 1800 MHz, and 2270 MHz.

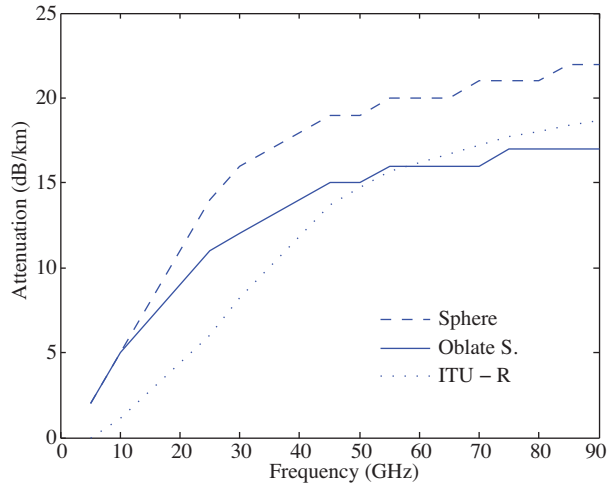


**Figure 6.** Comparison of attenuation of rain computation by using discrete model (sphere vs. oblate spheroid) and ITU-R rain model.

When Figure 6 is investigated in detail, it can be seen that although the oblate spheroid discrete model’s curve crosses the ITU-R rain model’s curve at one point, it does not reflect the characteristics of the ITU-R rain curve fully. Especially at frequencies lower than 50 GHz, the discrete model and the ITU-R model give very distinct results. On the other hand, the oblate spheroid model gives much better results compared to the sphere model since attenuation values are closer. To investigate which model fits best, percentage gaps were calculated and are given in Table 1.

As can be seen from Table 1, the sphere and the oblate spheroid produce very similar results up to 10 GHz; however, as the frequency is increased, the oblate spheroid model makes a better approximation and becomes closer to the ITU model. Sphere attenuation values calculated with the discrete model are always higher than the ITU-R model’s outcomes, whereas oblate spheroid attenuation calculated with the discrete model becomes smaller than the ITU-R model’s outcomes.

From computations of attenuation due to distorted raindrops for vertical and horizontal polarizations, the difference in attenuation from the values obtained for spherical particles is less than 16% for rain rates of up to 150 mm/h. This difference is small in comparison with the statistical variation of attenuation due to variations in drop-size distribution, and therefore the effects of departure from the perfect sphere shape can be ignored [10–12].

### 4.3. Simulation of snow attenuation

It has been mentioned that snow attenuation is more severe than attenuation in the case of rain due to large snowflake size and the composition of water, ice, and air molecules [12]. Therefore, careful investigation of snow attenuation should be done. However, there are some obstacles in predicting snow attenuation. First, there are many classifications of snowflake shapes, which are hard to determine and model. In most studies,

**Table 1.** Difference between ITU-R model and discrete model results in %.

Freq. (GHz)	Sphere gap (%)	Oblate gap (%)
5	1567	1567
10	238	238
15	145	115
20	117	78
25	99	57
30	79	34
35	58	21
40	46	13
45	39	10
50	28	1
55	27	1
60	21	-3
65	16	-7
70	18	-10
75	16	-6
80	13	-8
85	17	-10
90	15	-11

the shape of the snowflakes is assumed to be spherical or oblate spheroid, but these shapes fail to express the complex structure of snowflakes; therefore, expression of the theoretical analysis and phase shift is lacking [10–12]. Second, attenuation is predicted in 2 main ways: through scattering theory or empirically by using measurements. However, snowfalls are only seen occasionally, especially in places having tropical climate; therefore, a combined approach should be used for reliable information. Particle size, shape, and water content are the most important parameters in predicting snow attenuation. If snowflakes are categorized according to their water content, there are 2 limiting extremes: dry snow and wet snow. Mass density and particle size are inversely proportional, and they behave according to the formulas given in [10–12].

According to scientific research and experimentation, snowflake size ranges from 2 mm to 10 mm, whereas raindrop size ranges from 1 mm to 2 mm. Snowflake size also affects snow rate; as the size of the snowflake increases, the velocity of the particles also increases [16]. Snow attenuation was studied using a discrete model. Needles, plates, and branches, as seen in Table 2, are the main 3 groups of focus, and 13 different models were chosen as representative snow particles. The elements in each group were chosen according to similar characteristics of the ice crystals. In total, there are 4 groups to be investigated since plate group is divided into 2 because of similarities.

**Table 2.** Ice crystal groups.

Group Name	Ice Crystal Codes
Needles	N1a, N1c, N1e
Plate 1	P1a, P1c, P1e
Plate 2	P2a, P2g, P3b
Column	C1e, C1f, C1i, C1h

For each category, the diameter of the snowflake is estimated according to the studies done by Rasmussen et al. [14–16]. Moreover, relative length is determined for each ice crystal model according to the structure of

the model and the length/diameter ratio. Probability depicts the probability of finding that specific ice crystal among others in a snow cloud.

Simulation of snow-cloud modeling by using the discrete model was done and the attenuation levels compared to frequency and moisture content were obtained. Frequency was investigated at 3 distinct frequencies of 900 MHz, 1800 MHz, and 2270 MHz, since these are the frequencies that are commonly used for mobile communications in Turkey.

The density values were taken from previous studies [14–16] where rain modeling was done. Due to the fact that there are no estimations available that show the density of snowfall in Turkey, these values were used: moisture content: 0.7; distribution: uniform; length and diameter: changes according to each type given in shape, changes according to length, diameter, and ratio of ellipse axis.

When the simulation was run, results matching the expected results were gathered. The outcomes of the simulation can be seen in Figure 7. As can be observed, simulations of snow attenuation computation by using discrete modeling depict that as the frequency increases, attenuation levels increase drastically. However, there is no linear relation between frequency and attenuation: when the frequency is doubled from 900 MHz to 1800 MHz, attenuation increases approximately by half of the initial value, as was observed in rain attenuation simulation.

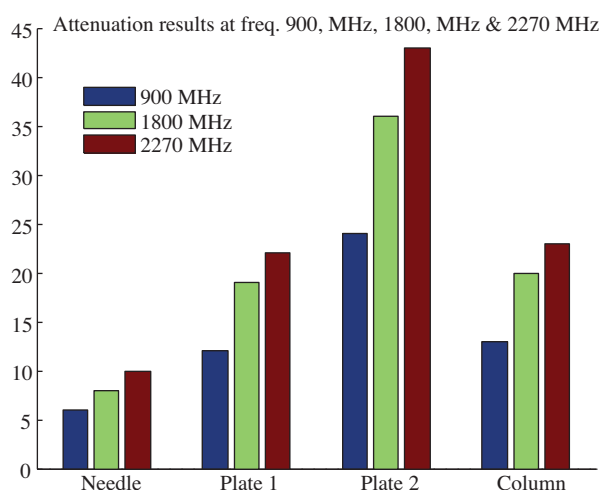


**Figure 7.** Snow attenuation at 900 MHz, 1800 MHz, and 2270 MHz.

When the attenuation levels of different crystal configurations were compared, results matched the expectations. Needle-type crystals were expected to have the lowest attenuation due to their geometry. Column-type and plane 1-type were expected to have similar results, which are higher than needle attenuation levels. Moreover, plane 2-type crystals would have a higher value of attenuation due to their higher moisture level, bigger size, and geometry.

In Section 2, it was observed that moisture content is also important for snow attenuation. It was proposed that it could create 2 degrees of magnitude difference in attenuation value due to increase in density. Therefore, attenuation values for different moisture levels were investigated in detail.

Input parameters for moisture: frequency: 2270 MHz (kept as high as possible to be able to observe changes clearly and chosen among the other ones used frequently in Turkey);

length: 0.50 m, diameter: 0.50 m, shape: sphere, distribution: uniform.

As can be observed clearly in Figure 8, attenuation and moisture have a direct relationship, as expected and as mentioned in the theory. In Figure 8, vertical and horizontal attenuation levels at different moisture content levels can also be seen. It should be noted that horizontal attenuation is very close to total attenuation, which means that it is more dominant in affecting total attenuation.

#### 4.4. Simulation of vegetation attenuation

Increasing the capacity and coverage of cellular communication systems requires a deeper understanding of how the environment surrounding the base station influences radio propagation. While considerable attention has been given in the literature to the influence of buildings [17–19], relatively few studies dealing with the effect of trees have been reported.

A realistic model for the propagation of electromagnetic waves in a vegetative environment has to consider that there is a more-or-less random distribution in the location, size, and possibly orientation of scattering elements. For the most part, the applicability of a given model is evaluated by comparing the model’s calculated attenuation to a measured value (of the same quantity). In this work, we used the above discrete approach for a multicomponent mobile propagation model of a park environment.

Mobile electromagnetic wave propagation through a park environment was studied by characterizing the media as a collection of discrete random scatterers. The electric fields in the park environment were represented by a mean (coherent) component.

The theoretical results along with experimental results, which were obtained by Bendix Co., USA, for both horizontal and vertical polarization were given in [19].

We calculated vertical polarized average power density and it was plotted against distance and attenuation. From Figure 9, as frequencies increase, power decays faster, and as attenuation increases, power decays faster.

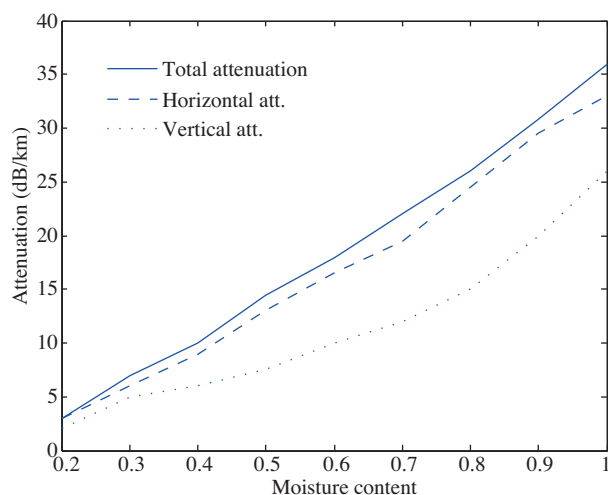


Figure 8. Snow attenuation at different moisture levels.

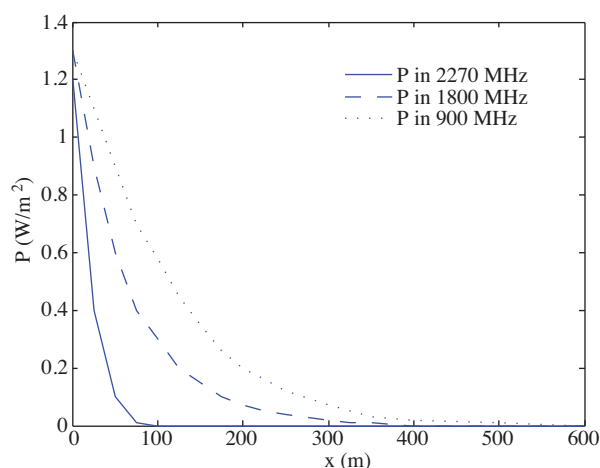


Figure 9. Vertical polarized average power density against distance.

#### 4.5. Conclusion

Simulation of the discrete model was attempted to provide a new approach to electromagnetic wave propagation through rain and snow. The formulation presented here offers several features. On the basis of our extensive

calculations, we may summarize our observations, some of which are already known. The formulation, being stochastic in nature, easily accommodates arbitrary polarization states and is valid for all frequency regions in which the criteria are satisfied. Complete characterization of the medium (e.g., attenuation, isolation, and phase shift) can be attained. Scattering particle distributions of size, shape, and orientation angle are directly included in the model. Variation of the medium density along the propagation path can be accommodated. The stochastic model yields less depolarization than does its deterministic counterpart, but comparison with experimental results reveals good agreement.

Finally, these results can be used to improve the interpretation of measured results from present rain and snow probing systems or to guide the design and deployment of future system margins and availability. It is hoped that the methods given in this work may provide a basis for the study of media in the millimeter wavelength. The numerical methods have been shown to be valid for the ranges of interest in these applications. The discrete model was applied by using oblate spheroid raindrop modeling, and it has been shown that oblate spheroid modeling of raindrops produces results that are more compatible with ITU-R results, especially when frequency exceeds 50 GHz.

In the further analysis of snow attenuation, it has been shown that for uniform distribution, attenuation due to snow is much more effective than attenuation due to rain. This is mostly because of the fact that snow has a bigger size. Needle-type snowflakes cause less attenuation than most of the other snowflakes, and certain plate-type snowflakes cause the highest attenuation levels. Moreover, attenuation due to snow increases as the moisture content of snowflakes increases.

In this work, only uniform distribution was used. Other distribution methods such as exponential distribution could be investigated in detail.

In both parts of the study, raindrops and snowflakes of a limited number of diameters were investigated. The scope of diameter could be enlarged and more simulations with different diameters could be observed.

Comparison of the discrete model with the snow attenuation model could not be done. The ITU does not recommend any specific regulation for snow attenuation, and for this reason, further investigation is needed.

From our analysis, we have seen that horizontal waves penetrate into vegetation more deeply than vertical waves. This is due primarily to the increasing attenuation that vertical waves suffer during propagation through the forest. In general, these losses are found to increase with frequency and to be dependent on the characteristics of the forest biomass. The rate of attenuation varies with the density of the woods, leaves, and branches and with the moisture content of vegetation. This study shows the difference between path losses at 2270, 1800, and 900 MHz, such that the loss is higher for a higher frequency range.

## Acknowledgment

This work was supported by the Boğaziçi University Research Foundation under Project Number 5698 and by the Marmara University Research Foundation under Project Number FEN-A-110412-0111. The authors would like to thank M Binme for her valuable help.

## References

- [1] International Telecommunication Union, ITU-R Recommendations 838, Specific Attenuation Model for Use in Prediction Method, Propagation in Non-Ionized Media, Geneva, ITU, 1994.
- [2] R.K. Crane, *Electromagnetic Wave Propagation through Rain*, New York, Wiley Interscience, 1996.

- [3] M.F. Iskander, Z. Yun, “Propagation prediction models for wireless communication systems”, *IEEE Transactions on Microwave Theory*, Vol. 50, pp. 662–673, 2002.
- [4] R.H. Lang, S.S. Seker, D.M. LeVine, “Vector solution for the mean electromagnetic fields in a layer of random particles”, *Radio Science*, Vol. 21, pp. 771–786, 1986.
- [5] L.J. Ippolito, *Propagation Effects Handbook for Satellite Systems Design*, 3rd ed., Ashburn, VA, USA, Stanford Telecom ACS, 1999.
- [6] International Telecommunication Union, *ITU-R Recommendations, Attenuation Due to Clouds and Fog*, pp. 840-3, Geneva, ITU, 1994.
- [7] A. Dissanayake, J. Allnutt, F. Haidara, “Cloud attenuation modeling for SHF and EHF applications”, *International Journal of Satellite Communication*, Vol. 19, pp. 335–345, 2001.
- [8] J.S. Ojo, M.O. Ajewole, S.K. Sarkar, “Rain rate and rain attenuation prediction for satellite communication in Ku and Ka bands over Nigeria”, *Progress in Electromagnetics Research B*, Vol. 5, pp. 207–223, 2008.
- [9] A.R. Holt, R.J. Rummings, G.J.G. Upton, W.J. Bradford, “Rain rates, drop size information and precipitation type, obtained from one-way differential propagation phase and attenuation along a microwave link”, *Radio Science*, Vol. 43, RS5009-18, 2008.
- [10] M.A. Fares, S.C. Fares, C.A. Ventrice, “Attenuation of the electromagnetic waves due to moist and wet snow”, *Proceedings of the IEEE Southeast Con*, pp. 99–104, 2007.
- [11] M.S. Awan, P. Brandl, E. Leitgeb, F. Nadeem, L. Csugai-Horvath, R. Nebuloni, “Transmission of high data rate optical signals in fog and snow conditions”, *Wireless Vitae*, pp. 702–706, 2009.
- [12] A. Ishimaru, *Wave Propagation and Scattering in Random Media*, London, UK, Academic Press, 1978.
- [13] S.S. Seker, “Radar cross-section of thin dielectric bodies”, *IEE Proceedings Part H*, Vol. 4, pp. 305–307, 1986.
- [14] R.M. Rasmussen, J. Vivekanandan, J. Cole, B. Myers, C. Masters, “The estimation of snowfall rate using visibility”, *Journal of Applied Meteorology*, Vol. 38, pp. 1542–1563, 1999.
- [15] T. Tjelta, D. Bacon, “Predicting combined rain and wet snow attenuation on terrestrial links”, *IEEE Transactions on Antenna and Propagation*, Vol. 58, pp. 1677–1682, 2010.
- [16] C. Magono, C.W. Lee, “Meteorological classification of natural snow crystals”, *Journal of Faculty Science, Hokkaido University, Japan, Series VII*, Vol. 2, pp. 321–335, 1966.
- [17] J.R. Cesar, D. Bello, L. Gláucio, H.L. Bertoni, “Theoretical analysis and measurement results of vegetation effects on path loss for mobile cellular communication systems”, *IEEE Transactions on Vehicular Technology*, Vol. 49, pp. 1285–1292, 2000.
- [18] S.S. Seker, F.C. Kunter, “Multi-components mobile propagation model of park environment”, *IEEE Transaction on Magnetism*, Vol. 47, pp. 1494–1497, 2011.
- [19] S.S. Seker, “Multi-components discrete propagation model of forest”, *IEE Proceedings Part H*, Vol. 142, pp. 201–206, 1995.